Generalized mode-coupling theory for mixtures of Brownian particles

Vincent E. Debets [1,2] Chengjie Luo [1,2] Simone Ciarella [1,3] and Liesbeth M. C. Janssen [1,2,*]

[1] *Department of Applied Physics, Eindhoven University of Technology, P.O. Box 513, 5600 MB Eindhoven, The Netherlands*

[2] *Institute for Complex Molecular Systems, Eindhoven University of Technology, P.O. Box 513, 5600 MB Eindhoven, The Netherlands*

[3] *Laboratoire de Physique de l'Ecole Normale Supérieure, ENS, Université PSL, CNRS, Sorbonne Université, Université de Paris, F-75005 Paris, France*

(Received 13 August 2021; accepted 29 November 2021; published 17 December 2021)

Generalized mode-coupling theory (GMCT) has recently emerged as a promising first-principles theory to study the poorly understood dynamics of glass-forming materials. Formulated as a hierarchical extension of standard mode-coupling theory (MCT), it is able to systematically improve its predictions by including the exact dynamics of higher-order correlation functions into its hierarchy. However, in contrast to Newtonian dynamics, a fully generalized version of the theory based on Brownian dynamics is still lacking. To close this gap, we provide a detailed derivation of GMCT for colloidal mixtures obeying a many-body Smoluchowski equation. We demonstrate that a hierarchy of coupled equations can again be established and show that these, consistent with standard MCT, are *identical* to the ones obtained from Newtonian GMCT when taking the overdamped limit. Consequently, the nontrivial similarity between Brownian and Newtonian MCT is maintained for our multicomponent GMCT. As a proof of principle, we also solve the generalized mode-coupling equations for the binary Kob-Andersen Lennard-Jones mixture undergoing Brownian dynamics and confirm the improved predictive power of the theory upon using more levels of the GMCT hierarchy of equations.

DOI: 10.1103/PhysRevE.104.065302

I. INTRODUCTION

To this date, the physical mechanisms underlying the liquid-to-glass transition are still not fully comprehended. Since glassy dynamics manifests itself in numerous systems across different length scales, e.g., atomic and molecular liquids, polymers, colloids, granular materials, and even living cells [1–11], a better understanding of this process is pivotal to a wide range of research areas. The main problem, however, remains that when a material transitions from a liquid to a glassy or amorphous solid state, its viscosity or relaxation time shows a tremendous nonlinear growth, while its structure and related thermodynamic control parameters exhibit only minor differences [12,13]. Consequently, a successful theory for glassy dynamics not only needs to pick up on these subtle structural changes, but also has to adequately magnify them in order to accurately describe the dramatic dynamical slowdown.

One of the few first-principles-based theories that is at least partially capable of this task is mode-coupling theory (MCT) [1,14–17]. This theory requires solely the static structure factor as input; from this structural information alone, it is able to predict the intermediate scattering function and thus the full microscopic relaxation dynamics of many glass-forming materials with qualitative and sometimes even semiquantitative accuracy. Among its most notable successes are the prediction of two-step relaxation patterns, stretched exponentials, and universal scaling laws upon approaching the glass transition point [1,14–18].

Unfortunately, MCT often fails to reach full quantitative accuracy; the primary reason for this resides in the theory's ad hoc Gaussian factorization and disregard of higher-order correlation functions. In recent years so-called generalized mode-coupling theory (GMCT) has therefore been introduced as a means to limit the effect of this uncontrolled approximation, with results that improve upon predictions of standard MCT in a systematic, possibly convergent manner [19–28]. The basic notion of this theory is to develop separate equations of motion for higher-order correlation functions instead of immediately applying a factorization approximation at the lowest possible order. This results in a hierarchy of MCT-like equations [19–24,28]. So far, the explicit inclusion of more high-order correlators has been shown to significantly enhance predictions in comparison to MCT, and near-quantitative accuracy in the weakly supercooled regime has already been reached [20]. Moreover, the theory has no free parameters, still only uses the static structure factor as input, and has thus presented itself as a promising first-principles theory to study the dynamics of glass-forming materials.

However, most of the GMCT studies and the accompanying derivations have focused primarily on systems governed by Newtonian dynamics, while the few works based on Brownian dynamics are restricted to single-component systems and time-independent properties [26,27]. Considering that an appreciable number of studied glassy materials, including polydisperse colloidal suspensions, is comprised of particles experiencing overdamped dynamics, it becomes apparent that a complete GMCT framework for multicomponent systems governed by Brownian dynamics is desired. For standard MCT it is known that deriving the theory from either

*l.m.c.janssen@tue.nl

Newtonian or Brownian principles yields the same results [24,29]. This subtle and nontrivial equivalency might be attributed to the fact that in MCT all "fast" variables are projected out and the differences between overdamped and underdamped dynamics seem to be covered within these "fast" variables. Since GMCT retains this method of projecting out "fast" variables and only extends it to higher-order correlation functions, we expect the observed similarity to persist upon generalizing the theory, although this is not *a priori* evident.

In this work we seek to formally demonstrate this equivalency by deriving a generalized MCT for colloidal mixtures obeying a many-body Smoluchowski equation. Our work significantly extends earlier GMCT studies [26,27] by accounting both for the full time-dependence of the Brownian relaxation dynamics and for polydisperse or multiple-particle-species compositions. Below we first present our model system and briefly recap the results of standard MCT. Next we provide detailed derivations of the equations of motion for the four-point and six-point density correlation functions and their dependence on the higher-order six- and eight-point density correlation functions (via the memory kernels), respectively. We discuss the similarities between the developed equations of motion and the lowest order MCT equation of motion and, based on them, extract a hierarchy of equations describing correlation functions of arbitrary order, thereby establishing a generalized MCT for mixtures of Brownian particles. A comparison is then made between Newtonian and Brownian GMCT, which are shown to be identical after taking the overdamped limit of the former. As a proof of principle, we also employ our theory to study some features, primarily the critical temperature, of the Kob-Andersen binary Lennard-Jones mixture [30]. This model system has been extensively studied in the context of glassy physics, and earlier comparisons with MCT have shown that the theory strongly overestimates the critical temperature [24,31–33]. We confirm the improved predictive power of GMCT by demonstrating that, upon including more levels of the hierarchy of equations, the critical temperature lowers in a possibly convergent manner towards the simulation results.

II. THEORY

A. Brownian particles

Our model glassy system is an m-component mixture consisting of N interacting spherical Brownian particles immersed in a viscous medium with total volume V. Following prior works on colloidal glasses, we neglect hydrodynamic interactions, so that the equation of motion for each particle is written as [32]

$$\frac{d\mathbf{r}_i^\alpha}{dt} = \zeta_\alpha^{-1}\mathbf{F}_i^\alpha + \boldsymbol{\xi}_i^\alpha. \tag{1}$$

Here, $\mathbf{r}_i^\alpha$ denotes the position of the ith particle of type α, $\mathbf{F}_i^\alpha$ the interaction force acting on it, ζ_α the component-dependent friction constant, and $\boldsymbol{\xi}_i^\alpha$ a Gaussian thermal noise with zero mean and variance $\langle \boldsymbol{\xi}_i^\alpha(t)\boldsymbol{\xi}_j^\beta(t')\rangle_{\text{noise}} = 2D^\alpha \mathbf{I}\delta_{ij}\delta_{\alpha\beta}\delta(t-t')$, with D^α the thermal diffusion coefficient, t the time, $\delta(t)$ the Dirac delta function, δ_{ij} the Kronecker delta, and $\mathbf{I}$ the unit matrix. Based on these equations the joint N-particle probability density function (PDF) evolves in time via [29,34]

$$\frac{\partial}{\partial t}P_N(\mathbf{r}^N, t) = \Omega P_N(\mathbf{r}^N, t), \tag{2}$$

where $\mathbf{r}^N = (\mathbf{r}_1^1, ..., \mathbf{r}_{N_m}^m)$ denotes the configuration space, and the evolution (or Smoluchowski) operator Ω is given by

$$\Omega = \sum_{\alpha=1}^{m}\sum_{i=1}^{N_\alpha} D^\alpha \nabla_i^\alpha \cdot \left(\nabla_i^\alpha - \beta\mathbf{F}_i^\alpha\right), \tag{3}$$

with N_α the number of particles of type α and β the inverse thermal energy. In equilibrium the PDF yields the Boltzmann solution $P_{\text{eq}}(\mathbf{r}^N) \propto \exp(-\beta U(\mathbf{r}^N))$. This solution depends solely on the total interaction potential $U(\mathbf{r}^N)$, which is spherically symmetric and produces the interaction forces $\mathbf{F}_i^\alpha = -\nabla_i^\alpha U(\mathbf{r}^N)$. Moreover, the friction constant and inverse thermal energy are related to each other via the Stokes-Einstein equation: $\beta D^\alpha = \zeta_\alpha^{-1}$. Note that D^α represents the intrinsic short-time diffusivity of the particles and should not be confused with the long-time diffusion coefficient, which may in fact violate the Stokes-Einstein equation upon approaching the glass transition point [18,32,35–37].

The collective motion of particles can then be described via density modes

$$\rho_\alpha(\mathbf{k}) = \frac{1}{\sqrt{N_\alpha}}\sum_{j=1}^{N_\alpha} e^{i\mathbf{k}\cdot\mathbf{r}_j^\alpha}, \tag{4}$$

where $\mathbf{k}$ is a wave vector and the factor $1/\sqrt{N_\alpha}$ is added for normalization. Our main probes to study the cooperative diffusion and glassy behavior of the colloids are the so-called partial intermediate scattering functions, which are the time correlation between two such density modes:

$$F_{\alpha;\beta}(k,t) = \langle \rho_\alpha^*(\mathbf{k}) e^{\Omega t}\rho_\beta(\mathbf{k})\rangle. \tag{5}$$

Note that they only depend on the absolute value $k = |\mathbf{k}|$ due to the system being isotropic and that, as a result of translational invariance, they are nonzero only when the wave vectors in both density modes are equal. At time zero the time correlation in Eq. (5) defines the static structure factor:

$$F_{\alpha;\beta}(k, t=0) \equiv S_{\alpha;\beta}(k) = \langle \rho_\alpha^*(\mathbf{k})\rho_\beta(\mathbf{k})\rangle. \tag{6}$$

We point out that averaging $\langle ...\rangle$ is done with respect to the equilibrium distribution $P_{\text{eq}}(\mathbf{r}^N)$ and that the operator Ω works on everything to its right including the PDF.

B. Mori-Zwanzig formalism

The framework of GMCT will be shown to consist of a hierarchy of equations of motion for $F_{\alpha;\beta}(k,t)$ and its higher-order counterparts. To obtain an equation of motion for such correlation functions we will employ the Mori-Zwanzig projector operator formalism [38,39], which we briefly summarize here. Consider any vector $\mathbf{A}$ whose elements $A_i = [\mathbf{A}]_i$ are functions of the configuration space $\mathbf{r}^N$ and whose time correlation is given by $\mathbf{F}(t) = \langle \mathbf{A}^* e^{\Omega t}\mathbf{A}\rangle$ or equivalently, in the Laplace domain $\mathbf{F}(z) = \langle \mathbf{A}^*(z-\Omega)^{-1}\mathbf{A}\rangle$. One can then define a projection operator onto the subspace spanned by $\mathbf{A}$ as $\mathcal{P} = |A_i\rangle S_{i;j}^{-1}\langle A_j^*|$, where we have adopted the Einstein summation convention to sum over repeated indices, introduced $\mathbf{S} = \langle \mathbf{A}^*\mathbf{A}\rangle$, and the superscript -1 denotes the inverse

matrix of the respective quantity, i.e., $S^{-1}_{i;j} \equiv [\mathbf{S}^{-1}]_{i;j}$. Note that the normalization $S^{-1}_{i;j}$ ensures the idempotency of $\mathcal{P}$. Typically, the elements in $\mathbf{A}$ are chosen to be slow or quasiconserved variables, which implies that $\mathcal{P}$ only retains the slow part parallel to $\mathbf{A}$, while removing the orthogonal or fast part. Invoking Dyson decomposition, i.e., $(z-\Omega)^{-1} = (z-\Omega\mathcal{Q})^{-1} + (z-\Omega\mathcal{Q})^{-1}\Omega\mathcal{P}(z-\Omega)^{-1}$, with $\mathcal{Q} = \mathcal{I} - \mathcal{P}$, one can write the Laplace transform of the time derivative of $\mathbf{F}(t)$ as

$$z\mathbf{F}(z) - \mathbf{S} = \langle \mathbf{A}^* \Omega(\mathcal{P}+\mathcal{Q})(z-\Omega)^{-1}\mathbf{A}\rangle = -\mathbf{H}\cdot\mathbf{S}^{-1}\cdot\mathbf{F}(z) + \mathbf{K}(z)\cdot\mathbf{S}^{-1}\cdot\mathbf{F}(z), \quad (7)$$

where we have introduced $\mathbf{H} = \langle \mathbf{A}^*\Omega\mathbf{A}\rangle$ and $\mathbf{K}(z) = \langle \mathbf{A}^*\Omega\mathcal{Q}(z-\mathcal{Q}\Omega\mathcal{Q})^{-1}\mathcal{Q}\Omega\mathbf{A}\rangle$, which are normally referred to as the diffusion matrix and the memory kernel, respectively. However, in its present form the memory kernel will not lend itself to MCT-like approximations [40,41]. We therefore follow standard procedure by converting it to an irreducible memory kernel. Employing a further projection operator $\mathcal{P}_{\rm irr} = |A_i\rangle H^{-1}_{i;j}\langle A^*_j\Omega|$, with $\mathcal{Q}_{\rm irr} = \mathcal{I} - \mathcal{P}_{\rm irr}$, and again invoking Dyson decomposition, we find that $\mathbf{K}(z) = \mathbf{M}(z) - \mathbf{M}(z)\cdot\mathbf{H}^{-1}\cdot\mathbf{K}(z)$. Here the irreducible memory kernel and evolution operator are given by $\mathbf{M}(z) = \langle \mathbf{A}^*\Omega\mathcal{Q}(z-\Omega_{\rm irr})^{-1}\mathcal{Q}\Omega\mathbf{A}\rangle$ and $\Omega_{\rm irr} = \mathcal{Q}\Omega\mathcal{Q}_{\rm irr}\mathcal{Q}$, respectively. By combining the relation between both memory kernels and Eq. (7), one arrives at

$$(\mathbf{I} + \mathbf{M}(z)\cdot\mathbf{H}^{-1})\cdot(z\mathbf{F}(z) - \mathbf{S}) + \mathbf{H}\cdot\mathbf{S}^{-1}\cdot\mathbf{F}(z) = 0. \quad (8)$$

If we then convert back to the time domain, we find an equation of motion for our correlation function $\mathbf{F}(t)$, which is given by

$$\frac{\partial}{\partial t}\mathbf{F}(t) + \mathbf{H}\cdot\mathbf{S}^{-1}\cdot\mathbf{F}(z) + \int_0^t \mathbf{M}(t-t')\cdot\mathbf{H}^{-1}\cdot\frac{\partial}{\partial t'}\mathbf{F}(t') = 0. \quad (9)$$

We mention that this equation is exact, although the memory kernel, which is usually the self-correlation function of so-called fluctuating forces, is often highly nontrivial and requires approximations to be evaluated.

In this work we shall take the density modes $\rho_\alpha(\mathbf{k})$, or any higher-order (multilinear) combination of density modes, as our dynamic variables A_i of interest. The Mori-Zwanzig approach then allows us to immediately develop a formally exact equation of motion for its time-correlation function. For the memory kernel we will invoke generalized MCT-based approximations to ultimately obtain a fully self-consistent set of equations. The derivation of this theory will be outlined below, and more explicit derivations are also included in the Supplemental Material [42].

C. Mode-coupling theory

Let us first consider the standard MCT framework for Brownian dynamics. Applying the Mori-Zwanzig projector operator formalism with $A_i = \rho_\alpha(\mathbf{k})$, the time evolution of $F_{\alpha;\beta}(k,t)$ is given by the following equation [29,32,43]:

$$\frac{\partial}{\partial t}F_{\alpha;\beta}(k,t) + H_{\alpha;\gamma}(k)S^{-1}_{\gamma;\epsilon}(k)F_{\epsilon;\beta}(k,t) + \int_0^t dt' M_{\alpha;\gamma}(k,t-t')H^{-1}_{\gamma;\epsilon}(k)\frac{\partial}{\partial t'}F_{\epsilon;\beta}(k,t') = 0, \quad (10)$$

where the collective two-point diffusion matrix governing the short-time dynamics is given by

$$H_{\alpha;\beta}(k) = -\langle \rho^*_\alpha(\mathbf{k})\Omega\rho_\beta(\mathbf{k})\rangle = k^2 D^\alpha \delta_{\alpha\beta}. \quad (11)$$

The crucial term of Eq. (10) is the irreducible two-point memory kernel $M_{\alpha;\beta}(k,t)$, which contains the time-autocorrelation function of the fluctuating forces. In MCT, these fluctuating forces are projected onto the subspace of density doublets, which are assumed to be the slowest modes after the single-density modes [16]. We mention that for Brownian systems such a projection is exact, since stress fluctuations can be expressed by pair densities [44]. By subsequently invoking the convolution approximation [45] and Gaussian factorization [20] for the three- and four-point static density correlations, respectively, which should be reasonable for systems not prone to form networks [46], the memory kernel can be written as [29,43]

$$M_{\alpha;\beta}(k,t) = \frac{1}{4}\sum_{\mathbf{q},\mathbf{q}'}\frac{D^\alpha}{\sqrt{N_\alpha}}V^\alpha_{\mu\nu}(\mathbf{k},\mathbf{q})\langle\rho^*_\mu(\mathbf{q})\rho^*_\nu(\mathbf{k}-\mathbf{q})e^{\Omega_{\rm irr}t} \times \rho_{\mu'}(\mathbf{q}')\rho_{\nu'}(\mathbf{k}-\mathbf{q}')\rangle\frac{D^\beta}{\sqrt{N_\beta}}V^\beta_{\mu'\nu'}(\mathbf{k},\mathbf{q}'), \quad (12)$$

with $\Omega_{\rm irr}$ representing the irreducible evolution operator [29,40,41,43]. The vertices, which represent the coupling strength between different wave vectors, are written in terms of the direct correlation function $C_{\alpha\beta}(k) = \delta_{\alpha\beta} - S^{-1}_{\alpha\beta}(k)$ as

$$V^\alpha_{\mu\nu}(\mathbf{k},\mathbf{q}) = \mathbf{k}\cdot\mathbf{q}\,\delta_{\alpha\nu}C_{\alpha\mu}(q) + \mathbf{k}\cdot(\mathbf{k}-\mathbf{q})\,\delta_{\alpha\mu}C_{\alpha\nu}(|\mathbf{k}-\mathbf{q}|). \quad (13)$$

It is apparent that the irreducible two-point memory kernel requires an even more complex (unknown) irreducible four-point dynamic density correlation, which prevents one from finding numerical solutions. Approximations are therefore desired, and in standard MCT this takes the shape of an ad hoc factorization. In particular, the irreducible evolution operator $\Omega_{\rm irr}$ is replaced by the full time-evolution operator Ω, and the four-point density correlations are written as products of two-point density correlations, yielding [29,43]

$$\langle\rho^*_\mu(\mathbf{q})\rho^*_\nu(\mathbf{k}-\mathbf{q})e^{\Omega^{\rm irr}t}\rho_{\mu'}(\mathbf{q}')\rho_{\nu'}(\mathbf{k}-\mathbf{q}')\rangle \approx F_{\mu;\mu'}(q,t)F_{\nu;\nu'}(|\mathbf{k}-\mathbf{q}|,t)\delta_{\mathbf{q},\mathbf{q}'} + F_{\mu;\nu'}(q,t)F_{\nu;\mu'}(|\mathbf{k}-\mathbf{q}|,t)\delta_{\mathbf{k}-\mathbf{q},\mathbf{q}'}. \quad (14)$$

Consequently, the irreducible two-point memory kernel simplifies to [29]

$$M_{\alpha;\beta}(k,t) = \frac{1}{2}\sum_{\mathbf{q}}\frac{D^\alpha}{\sqrt{N_\alpha}}V^\alpha_{\mu\nu}(\mathbf{k},\mathbf{q})F_{\mu;\mu'}(q,t) \times F_{\nu;\nu'}(|\mathbf{k}-\mathbf{q}|,t)\frac{D^\beta}{\sqrt{N_\beta}}V^\beta_{\mu'\nu'}(\mathbf{k},\mathbf{q}), \quad (15)$$

which, using the static structure factor $F_{\alpha;\beta}(k, t = 0) = S_{\alpha;\beta}(k)$ as the initial boundary condition, allows us to self-consistently find a solution for $F_{\alpha;\beta}(k, t)$ and study the glassy dynamics of our colloidal mixture.

D. Extending towards generalized mode-coupling theory

Despite the remarkable successes of MCT [1,16,18,47], several discrepancies between the theory and simulations or experiments still persist [31,48–50], most notably, an overestimation of the glass transition. Inspired by previous studies [19–27], we therefore seek to improve and generalize the theory by developing a separate equation for the four-point dynamic density correlations (and later continuing the process for even higher-order correlations). Since we believe the factorization to be the most severe approximation, we will retain the four-point density correlations and only replace the irreducible evolution operator by a full one. Moreover, to keep calculations tractable and consistent with previous work on Newtonian GMCT, we will also apply the diagonal approximation ($\mathbf{q} = \mathbf{q}', \mathbf{k} - \mathbf{q} = \mathbf{q}'$) [20,22,23,51], so that overall we have

$$\begin{aligned}\langle \rho^*_\mu(\mathbf{q})\rho^*_\nu(\mathbf{k}-\mathbf{q})e^{\Omega^{\mathrm{irr}}t}\rho_{\mu'}(\mathbf{q}')\rho_{\nu'}(\mathbf{k}-\mathbf{q}')\rangle \\ \approx F^{(2)}_{\mu\nu;\mu'\nu'}(q,|\mathbf{k}-\mathbf{q}|,t)\delta_{\mathbf{q},\mathbf{q}'}+F^{(2)}_{\mu\nu;\nu'\mu'}(q,|\mathbf{k}-\mathbf{q}|,t)\delta_{\mathbf{k}-\mathbf{q},\mathbf{q}'}.\end{aligned} \tag{16}$$

As a result, the memory kernel becomes a function of the diagonal four-point dynamic density correlation function $F^{(2)}_{\alpha_1\alpha_2;\beta_1\beta_2}(k_1, k_2, t) = \langle \rho^*_{\alpha_1}(\mathbf{k}_1)\rho^*_{\alpha_2}(\mathbf{k}_2)e^{\Omega t}\rho_{\beta_1}(\mathbf{k}_1)\rho_{\beta_2}(\mathbf{k}_2)\rangle$:

$$\begin{aligned}M_{\alpha;\beta}(k,t) = \frac{1}{2}\sum_{\mathbf{q}}\frac{D^\alpha}{\sqrt{N_\alpha}}V^\alpha_{\mu\nu}(\mathbf{k},\mathbf{q}) \\ \times F^{(2)}_{\mu\nu;\mu'\nu'}(q,|\mathbf{k}-\mathbf{q}|,t)\frac{D^\beta}{\sqrt{N_\beta}}V^\beta_{\mu'\nu'}(\mathbf{k},\mathbf{q}).\end{aligned} \tag{17}$$

Having simplified the irreducible to a diagonal four-point density correlation, we can now once more resort to the Mori-Zwanzig projection operator formalism to describe its dynamics. Using $A_i = \rho_{\alpha_1}(\mathbf{k}_1)\rho_{\alpha_2}(\mathbf{k}_2)$ in Eq. (9), the equation of motion for the four-point density correlation function yields

$$\begin{aligned}&\frac{\partial}{\partial t}F^{(2)}_{\alpha_1\alpha_2;\beta_1\beta_2}(k_1,k_2,t) + H^{(2)}_{\alpha_1\alpha_2;\gamma_1\gamma_2}(k_1,k_2)\big(S^{(2)}\big)^{-1}_{\gamma_1\gamma_2;\epsilon_1\epsilon_2}(k_1,k_2)\,F^{(2)}_{\epsilon_1\epsilon_2;\beta_1\beta_2}(k_1,k_2,t) \\ &\quad + \int_0^t dt' M^{(2)}_{\alpha_1\alpha_2;\gamma_1\gamma_2}(k_1,k_2,t-t')\big(H^{(2)}\big)^{-1}_{\gamma_1\gamma_2;\epsilon_1\epsilon_2}(k_1,k_2)\,\frac{\partial}{\partial t'}F^{(2)}_{\epsilon_1\epsilon_2;\beta_1\beta_2}(k_1,k_2,t') = 0.\end{aligned} \tag{18}$$

In this equation the collective diffusion matrix and static structure factor are naturally extended towards their four-point tensorial counterparts:

$$\begin{aligned}H^{(2)}_{\alpha_1\alpha_2;\beta_1\beta_2}(k_1,k_2) &= -\big\langle \rho^*_{\alpha_1}(\mathbf{k}_1)\rho^*_{\alpha_2}(\mathbf{k}_2)\Omega\rho_{\beta_1}(\mathbf{k}_1)\rho_{\beta_2}(\mathbf{k}_2)\big\rangle \\ &= k_1^2 D^{\alpha_1}\delta_{\alpha_1\beta_1}S_{\alpha_2;\beta_2}(k_2) + k_2^2 D^{\alpha_2}\delta_{\alpha_2\beta_2}S_{\alpha_1;\beta_1}(k_1),\end{aligned} \tag{19}$$

and

$$\begin{aligned}S^{(2)}_{\alpha_1\alpha_2;\beta_1\beta_2}(k_1,k_2) &= \big\langle \rho^*_{\alpha_1}(\mathbf{k}_1)\rho^*_{\alpha_2}(\mathbf{k}_2)\rho_{\beta_1}(\mathbf{k}_1)\rho_{\beta_2}(\mathbf{k}_2)\big\rangle \\ &\approx S_{\alpha_1;\beta_1}(k_1)S_{\alpha_2;\beta_2}(k_2),\end{aligned}$$

where the latter is approximated using Gaussian factorization, which, from this point onward, will be done throughout for static correlations. Moreover, the four-point irreducible memory kernel reads

$$M^{(2)}_{\alpha_1\alpha_2;\beta_1\beta_2}(k_1,k_2,t) = \big\langle \rho^*_{\alpha_1}(\mathbf{k}_1)\rho^*_{\alpha_2}(\mathbf{k}_2)\Omega\mathcal{Q}^{(2)}e^{\Omega^{(2)}_{\mathrm{irr}}t}\mathcal{Q}^{(2)}\Omega\rho_{\beta_1}(\mathbf{k}_1)\rho_{\beta_2}(\mathbf{k}_2)\big\rangle. \tag{20}$$

Unfortunately, the complexity of the latter term hinders any analytical progress, and our strategy to develop Brownian-GMCT is therefore to simplify it by invoking a similar strategy as is done in MCT. Realizing that the second-order fluctuating forces consist, to leading order, of products of three density modes [20,26], we seek to project the second-order fluctuating forces onto the subset of density triplets. More concretely, this translates to replacing $\langle \rho^*_{\alpha_1}(\mathbf{k}_1)\rho^*_{\alpha_2}(\mathbf{k}_2)\Omega\mathcal{Q}^{(2)} \to \langle \rho^*_{\alpha_1}(\mathbf{k}_1)\rho^*_{\alpha_2}(\mathbf{k}_2)\Omega\mathcal{Q}^{(2)}\mathcal{P}_3$ and $\mathcal{Q}^{(2)}\Omega\rho_{\beta_1}(\mathbf{k}_1)\rho_{\beta_2}(\mathbf{k}_2)\rangle \to \mathcal{P}_3\mathcal{Q}^{(2)}\Omega\rho_{\beta_1}(\mathbf{k}_1)\rho_{\beta_2}(\mathbf{k}_2)\rangle$ in the four-point irreducible memory kernel using the projection operator

$$\mathcal{P}_3 = \frac{1}{6}\sum_{\mathbf{q}_1,\mathbf{q}_2,\mathbf{q}_3}\big|\rho_{\mu_1}(\mathbf{q}_1)\rho_{\mu_2}(\mathbf{q}_2)\rho_{\mu_3}(\mathbf{q}_3)\big\rangle\chi_{123}\big\langle\rho^*_{\nu_1}(\mathbf{q}_1)\rho^*_{\nu_2}(\mathbf{q}_2)\rho^*_{\nu_3}(\mathbf{q}_3)\big|. \tag{21}$$

Note that the factor $1/6$ corrects for double counting and that the normalization $\chi_{123} = S^{-1}_{\mu_1;\nu_1}(q_1)S^{-1}_{\mu_2;\nu_2}(q_2)S^{-1}_{\mu_3;\nu_3}(q_3)$ is chosen in accordance with Gaussian factorization. Due to this projection, the memory kernel takes on the more familiar form of two "vertices" enclosing a correlation one step above in the hierarchy, which in this case is a six-point irreducible correlation function:

$$\begin{aligned}M^{(2)}_{\alpha_1\alpha_2;\beta_1\beta_2}(k_1,k_2,t) \approx \frac{1}{36}\sum_{\mathbf{q}_1\ldots\mathbf{q}_6}\big\langle \rho^*_{\alpha_1}(\mathbf{k}_1)\rho^*_{\alpha_2}(\mathbf{k}_2)\Omega\mathcal{Q}^{(2)}\rho_{\mu_1}(\mathbf{q}_1)\rho_{\mu_2}(\mathbf{q}_2)\rho_{\mu_3}(\mathbf{q}_3)\big\rangle\chi_{123} \\ \times\big\langle\rho^*_{\nu_1}(\mathbf{q}_1)\rho^*_{\nu_2}(\mathbf{q}_2)\rho^*_{\nu_3}(\mathbf{q}_3)e^{\Omega^{(2)}_{\mathrm{irr}}t}\rho_{\mu_4}(\mathbf{q}_4)\rho_{\mu_5}(\mathbf{q}_5)\rho_{\mu_6}(\mathbf{q}_6)\big\rangle\chi_{456}\big\langle\rho^*_{\nu_4}(\mathbf{q}_4)\rho^*_{\nu_5}(\mathbf{q}_5)\rho^*_{\nu_6}(\mathbf{q}_6)\mathcal{Q}^{(2)}\Omega\rho_{\beta_1}(\mathbf{k}_1)\rho_{\beta_2}(\mathbf{k}_2)\big\rangle.\end{aligned} \tag{22}$$

Following the detailed derivation reported in the Supplemental Material [42], it is possible to reduce the left vertex to

$$\begin{aligned}&\left\langle\rho^*_{\alpha_1}(\mathbf{k}_1)\rho^*_{\alpha_2}(\mathbf{k}_2)\Omega\mathcal{Q}^{(2)}\rho_{\mu_1}(\mathbf{q}_1)\rho_{\mu_2}(\mathbf{q}_2)\rho_{\mu_3}(\mathbf{q}_3)\right\rangle\chi_{123}\\&=\Bigg[\left(\frac{D^{\alpha_1}}{\sqrt{N_{\alpha_1}}}\delta_{\mathbf{k}_1,\mathbf{q}_1+\mathbf{q}_2}\delta_{\mathbf{k}_2,\mathbf{q}_3}\delta_{\alpha_2\nu_3}\left(k_1^2\delta_{\alpha_1\nu_1}\delta_{\alpha_1\nu_2}-\mathbf{k}_1\cdot\mathbf{q}_1\delta_{\alpha_1\nu_2}S^{-1}_{\alpha_1;\nu_1}(q_1)-\mathbf{k}_1\cdot\mathbf{q}_2\delta_{\alpha_1\nu_1}S^{-1}_{\alpha_1;\nu_2}(q_2)\right)\right)\\&\quad+(\{\mathbf{q}_1,\nu_1\leftrightarrow\mathbf{q}_3,\nu_3\})+(\{\mathbf{q}_2,\nu_2\leftrightarrow\mathbf{q}_3,\nu_3\})\Bigg]+[\{\mathbf{k}_1,\alpha_1\leftrightarrow\mathbf{k}_2,\alpha_2\}],\end{aligned}\tag{23}$$

while the right vertex yields an identical expression. Here, the double-arrow contributions correspond to the aforementioned terms enclosed by the same brackets except for a swapping of the indicated wave vectors and particle labels. Inserting both results, evaluating the Kronecker deltas, and exploiting the symmetry of the different vertex terms allows us to rewrite the memory kernel as

$$\begin{aligned}&M^{(2)}_{\alpha_1\alpha_2;\beta_1\beta_2}(k_1,k_2,t)\\&\approx\frac{1}{4}\sum_{\mathbf{q},\mathbf{q}'}\Bigg[\frac{D^{\alpha_1}}{\sqrt{N_{\alpha_1}}}V^{\alpha_1}_{\mu\nu}(\mathbf{k}_1,\mathbf{q})\Bigg(\left\langle\rho^*_\mu(\mathbf{q})\rho^*_\nu(\mathbf{k}_1-\mathbf{q})\rho^*_{\alpha_2}(\mathbf{k}_2)e^{\Omega^{(2)}_{\mathrm{irr}}t}\rho_{\mu'}(\mathbf{q}')\rho_{\nu'}(\mathbf{k}_1-\mathbf{q}')\rho_{\beta_2}(\mathbf{k}_2)\right\rangle\frac{D^{\beta_1}}{\sqrt{N_{\beta_1}}}V^{\beta_1}_{\mu'\nu'}(\mathbf{k}_1,\mathbf{q}')\\&\quad+\left\langle\rho^*_\mu(\mathbf{q})\rho^*_\nu(\mathbf{k}_1-\mathbf{q})\rho^*_{\alpha_2}(\mathbf{k}_2)e^{\Omega^{(2)}_{\mathrm{irr}}t}\rho_{\mu'}(\mathbf{q}')\rho_{\nu'}(\mathbf{k}_2-\mathbf{q}')\rho_{\beta_1}(\mathbf{k}_1)\right\rangle\frac{D^{\beta_2}}{\sqrt{N_{\beta_2}}}V^{\beta_2}_{\mu'\nu'}(\mathbf{k}_2,\mathbf{q}')\Bigg)\Bigg]+[\{\mathbf{k}_1,\alpha_1,\beta_1\leftrightarrow\mathbf{k}_2,\alpha_2,\beta_2\}],\end{aligned}\tag{24}$$

which is very reminiscent of (12) and therefore lends itself to similar approximations. In particular, we can again replace the irreducible operator with a full evolution operator and apply the diagonal approximation, which for second order comes down to $\mathbf{q}=\mathbf{q}'$, $\mathbf{k}_{1,2}-\mathbf{q}=\mathbf{q}'$, and retaining only diagonal correlations [20,22,23]. Combined with the assumption that $\mathbf{k}_1\neq\mathbf{k}_2$, the memory kernel finally reduces to

$$M^{(2)}_{\alpha_1\alpha_2;\beta_1\beta_2}(k_1,k_2,t)\approx\frac{1}{2}\sum_{\mathbf{q}}\left(\frac{D^{\alpha_1}}{\sqrt{N_{\alpha_1}}}V^{\alpha_1}_{\mu\nu}(\mathbf{k}_1,\mathbf{q})F^{(3)}_{\mu\nu\alpha_2;\mu'\nu'\beta_2}(q,|\mathbf{k}_1-\mathbf{q}|,k_2,t)\frac{D^{\beta_1}}{\sqrt{N_{\beta_1}}}V^{\beta_1}_{\mu'\nu'}(\mathbf{k}_1,\mathbf{q})\right)+(\{\mathbf{k}_1,\alpha_1,\beta_1\leftrightarrow\mathbf{k}_2,\alpha_2,\beta_2\}),\tag{25}$$

and thus becomes a function of the diagonal six-point density correlation:

$$F^{(3)}_{\alpha_1\alpha_2\alpha_3;\beta_1\beta_2\beta_3}(k_1,k_2,k_3,t)=\left\langle\rho^*_{\alpha_1}(\mathbf{k}_1)\rho^*_{\alpha_2}(\mathbf{k}_2)\rho^*_{\alpha_3}(\mathbf{k}_3)e^{\Omega t}\rho_{\beta_1}(\mathbf{k}_1)\rho_{\beta_2}(\mathbf{k}_2)\rho_{\beta_3}(\mathbf{k}_3)\right\rangle.\tag{26}$$

To recapitulate, we now have a set of two coupled equations for the two- and four-point density correlations, Eqs. (10) and (18), which can be solved self-consistently by using an approximate expression for the six-point density correlation function, using as input the static structure factor and the initial boundary conditions. Normally, this is done by factorizing the six-point correlation function in terms of its lower-order counterparts [20,26]. This system of two coupled equations constitutes a first improvement upon standard MCT, since it pushes the factorization approximation back to a higher-order correlation function, hence the name second-order GMCT.

E. Hierarchy of GMCT equations

We are, however, by no means forced to introduce a factorization at the level of the six-point density correlations. In fact, the entire process laid out for the four-point density correlation function can be equally repeated for the diagonal six-point density correlations. Using $A_i=\rho_{\alpha_1}(\mathbf{k}_1)\rho_{\alpha_2}(\mathbf{k}_2)\rho_{\alpha_3}(\mathbf{k}_3)$ in (9) yields an equivalent equation of motion for $F^{(3)}_{\alpha_1\alpha_2\alpha_3;\beta_1\beta_2\beta_3}(k_1,k_2,k_3,t)$ [see Eq. (S27)], which, after simplifying the irreducible six-point memory kernel, can be shown to depend on the diagonal eight-point density correlation functions (see Supplemental Material [42] for more details). An inspection of the simplified second [Eq. (25)] and third [Eq. (S33)] order irreducible memory kernels then shows that they are very similar and we may, in agreement with previous work on GMCT, observe a hierarchy of equations starting to unfold [19–24,28,52]. Extrapolating the observed behavior, we define a general $2n$ density correlation function,

$$\begin{aligned}&F^{(n)}_{\{\alpha_i\};\{\beta_i\}}(\{k_i\},t)\\&\quad=\left\langle\rho^*_{\alpha_1}(\mathbf{k}_1)\ldots\rho^*_{\alpha_n}(\mathbf{k}_n)e^{\Omega t}\rho_{\beta_1}(\mathbf{k}_1)\ldots\rho_{\beta_n}(\mathbf{k}_n)\right\rangle,\end{aligned}\tag{27}$$

which, using $A_i=\rho_{\alpha_1}(\mathbf{k}_1)\ldots\rho_{\alpha_n}(\mathbf{k}_n)$ in (9), obeys the following equation of motion:

$$\begin{aligned}&\frac{\partial}{\partial t}F^{(n)}_{\{\alpha_i\};\{\beta_i\}}(\{k_i\},t)+H^{(n)}_{\{\alpha_i\};\{\gamma_i\}}(\{k_i\})\\&\quad\times\left(S^{(n)}\right)^{-1}_{\{\gamma_i\};\{\delta_i\}}(\{k_i\})\,F^{(n)}_{\{\delta_i\};\{\beta_i\}}(\{k_i\},t)\\&\quad+\int_0^t d\tau M^{(n)}_{\{\alpha_i\};\{\gamma_i\}}(\{k_i\},\tau)(H^{(n)})^{-1}_{\{\gamma_i\};\{\delta_i\}}(\{k_i\})\\&\quad\times\frac{\partial}{\partial t}F^{(n)}_{\{\delta_i\};\{\beta_i\}}(\{k_i\},t-\tau)=0.\end{aligned}\tag{28}$$

Here $\{\alpha_i\}=\{\alpha_1,\ldots,\alpha_n\}$ and $\{k_i\}=\{k_1,\ldots,k_n\}$ denote sets of n particle labels and wave vectors, respectively, and the generalized static structure and collective diffusion tensors are

given by

$$S^{(n)}_{\{\alpha_i\};\{\beta_i\}}(\{k_i\}) = \left\langle \rho^*_{\alpha_1}(\mathbf{k}_1)\dots\rho^*_{\alpha_n}(\mathbf{k}_n)\rho_{\beta_1}(\mathbf{k}_1)\dots\rho_{\beta_n}(\mathbf{k}_n)\right\rangle \approx \prod_{i=1}^{n} S_{\alpha_i\beta_i}(k_i) \tag{29}$$

and

$$H^{(n)}_{\{\alpha_i\};\{\beta_i\}}(\{k_i\}) = -\left\langle \rho^*_{\alpha_1}(\mathbf{k}_1)\dots\rho^*_{\alpha_n}(\mathbf{k}_n)\Omega\rho_{\beta_1}(\mathbf{k}_1)\dots\rho_{\beta_n}(\mathbf{k}_n)\right\rangle = \sum_{i=1}^{n}\left(D_{\alpha_i}k_i^2\delta_{\alpha_i\beta_i}\prod_{j\neq i}S_{\alpha_j\beta_j}(k_j)\right),$$

respectively. Finally, using $\{\alpha_{i\neq j}\}$ to represent the set $\{\alpha_i\}$ without the element α_j, introducing the component-dependent number density $n_\alpha = N_\alpha/V$, and taking the thermodynamic limit, i.e., $\sum_{\mathbf{q}} \to \frac{V}{(2\pi)^3}\int d\mathbf{q}$, the generalized memory kernel may be written as

$$M^{(n)}_{\{\alpha_i\};\{\beta_i\}}(\{k_i\},t) = \int\frac{d\mathbf{q}}{16\pi^3}\left(\sum_{j=1}^{n}\frac{D^{\alpha_j}}{\sqrt{n_{\alpha_j}}}V^{\alpha_j}_{\mu\nu}(\mathbf{k}_j,\mathbf{q})F^{(n+1)}_{\mu\nu\{\alpha_{i\neq j}\};\mu'\nu'\{\beta_{i\neq j}\}} \times (q,|\mathbf{k}_j-\mathbf{q}|,\{k_{i\neq j}\},t)\frac{D^{\beta_j}}{\sqrt{n_{\beta_j}}}V^{\beta_j}_{\mu'\nu'}(\mathbf{k}_j,\mathbf{q})\right). \tag{30}$$

Note that $n = 1, 2, 3$ correspond to Eqs. (17), (25), and (S33), respectively (with the latter presented in the Supplemental Material) and that the memory kernel forms the link between each equation of motion and the next via its dependence on the $2(n+1)$ density correlation functions. Overall, we are now left with a hierarchy of connected integrodifferential equations which are subject to the initial boundary conditions $F^{(n)}_{\{\alpha_i\};\{\beta_i\}}(\{k_i\},t=0) = S^{(n)}_{\{\alpha_i\};\{\beta_i\}}(\{k_i\})$ and, in principle, can go up to arbitrary order in n. For computational reasons, however, one must close the hierarchy at a suitable order $n = n_{\max}$. Increasing the value of $n_{\max}$ pushes the factorization to higher-order correlation functions (see Sec. III for more details).

To summarize, we have demonstrated that a multicomponent GMCT formalism can be constructed for Brownian systems governed by a many-body Smoluchowski equation. A comparison of our presented results with recent work on multicomponent Newtonian GMCT [24] shows that in the overdamped limit both hierarchies of equations are completely identical. This demonstrates that the nontrivial similarity between Brownian and Newtonian systems witnessed for standard MCT is maintained for GMCT. Interestingly, this also implies that the equilibrium Smoluchowski operator in the equilibrium-distribution scalar product in Brownian GMCT essentially acts in an analogous manner as the double appearance of the Liouville operator in Newtonian GMCT.

F. Long-time limit

We finalize our discussion of the theory by mentioning that, based on the derived equations of motion, we can also formulate a relation for the long-time limit of the $2n$ density correlation functions or the so-called nonergodicity parameters f. Taking the Laplace transform of (28) and invoking the final value theorem, we have

$$H^{(n)}_{\{\alpha_i\};\{\gamma_i\}}(\{k_i\})(S^{(n)})^{-1}_{\{\gamma_i\};\{\delta_i\}}(\{k_i\})\,f^{(n)}_{\{\delta_i\};\{\beta_i\}}(\{k_i\}) + m^{(n)}_{\{\alpha_i\};\{\gamma_i\}}(\{k_i\})(H^{(n)})^{-1}_{\{\gamma_i\};\{\delta_i\}}(\{k_i\}) \times\left(f^{(n)}_{\{\delta_i\};\{\beta_i\}}(\{k_i\}) - S^{(n)}_{\{\delta_i\};\{\beta_i\}}(\{k_i\})\right) = 0, \tag{31}$$

where the long-time limits are defined as

$$f^{(n)}_{\{\alpha_i\};\{\beta_i\}}(\{k_i\}) = \lim_{t\to\infty} F^{(n)}_{\{\alpha_i\};\{\beta_i\}}(\{k_i\},t), \tag{32}$$

and

$$m^{(n)}_{\{\alpha_i\};\{\beta_i\}}(\{k_i\}) = \lim_{t\to\infty} M^{(n)}_{\{\alpha_i\};\{\beta_i\}}(\{k_i\},t) = \int\frac{d\mathbf{q}}{16\pi^3}\left(\sum_{j=1}^{n}\frac{D^{\alpha_j}}{\sqrt{n_{\alpha_j}}}V^{\alpha_j}_{\mu\nu}(\mathbf{k}_j,\mathbf{q}) f^{(n+1)}_{\mu\nu\{\alpha_{i\neq j}\};\mu'\nu'\{\beta_{i\neq j}\}}(q,|\mathbf{k}_j-\mathbf{q}|,\{k_{i\neq j}\})\frac{D^{\beta_j}}{\sqrt{n_{\beta_j}}}V^{\beta_j}_{\mu'\nu'}(\mathbf{k}_j,\mathbf{q})\right). \tag{33}$$

For the nonergodicity parameters we thus find a similar hierarchy of, in this case geometric equations, which must also be closed at a suitable order $n_{\max}$ to allow for the obtainment of practical results.

Finally, we mention that it is straightforwardly shown that the lowest order equation of this hierarchy is independent of the diffusivities D^α [53]. In other words, the location of the glass transition is independent of kinetic parameters in standard MCT. It is not immediately clear whether this also holds true for the higher-order equations, i.e., for GMCT. Interestingly, we have found that the critical temperatures for higher-order GMCT in this work seem to change when we vary the ratio between the different diffusion constants D^α while using the same structural input. We have also verified that this behavior is robust when choosing different mean-field closures. GMCT might therefore be better equipped to deal with asymmetric intrinsic diffusivities, which have been shown to influence long-time dynamics in binary mixtures [54], although for hard spheres they do not seem to influence the critical density [55].

III. NUMERICAL DETAILS

A. GMCT numerics

Our aim is to self-consistently solve the hierarchies of equations for different closure levels $n_{\max}$. To attain such solutions we will employ the following mean-field closure for $n_{\max} > 1$ [20,24]:

$$M^{(n_{\max})}_{\{\alpha_i\};\{\beta_i\}}(\{k_i\},t) \approx \frac{1}{n_{\max}-1}\sum_j M^{(n_{\max}-1)}_{\{\alpha_{i\neq j}\};\{\beta_{i\neq j}\}}(\{k_{i\neq j}\},t)F_{\alpha_j;\beta_j}(k_j,t), \tag{34}$$

where we have taken into account the invariance of $F^{(n)}_{\{\alpha_i\};\{\beta_i\}}(\{k_i\},t)$ under the exchange $\{k_i,\alpha_i,\beta_i \leftrightarrow k_j,\alpha_j,\beta_j\}$, and the factor $1/(n_{\max}-1)$ ensures that at $t=0$ both sides are equal under Gaussian factorization. Note that this closure

is equivalent to assuming $F^{(n_{\max}+1)}(t) \sim F^{(n_{\max})}(t) \times F^{(1)}(t)$ and is therefore consistent with the standard MCT approximation, i.e. (14), when setting $n_{\max} = 1$. Using these closures we find explicit expressions for all correlation functions up to $F^{(n_{\max})}_{\{\alpha_i\};\{\beta_i\}}(\{k_i\}, t)$, although we will concentrate mainly on $F^{(1)}$, which is usually measured in simulations and experiments. Moreover, by increasing the hierarchy level $n_{\max}$, the factorization approximation naturally gets shifted towards higher-order correlations $F^{(n_{\max}+1)}_{\{\alpha_i\};\{\beta_i\}}(\{k_i\}, t)$, which can systematically improve predictions for both single-component and binary systems [19–24,26,27].

Fixing the closure tells us how many integrodifferential equations to include, but we also require a numerical scheme to solve each of them. For this we exploit the system's rotational symmetry to rewrite the three-dimensional integral over $\mathbf{q}$ present in (30) in terms of two bipolar coordinates $q = |\mathbf{q}|$, $p = |\mathbf{k}_j - \mathbf{q}|$, which are subsequently approximated by a double Riemann sum [56] using an equidistant wave-vector grid $k\sigma = [0.2, 0.6, \ldots, 39.8]$ (with σ the unit of length). To retrieve solutions for the time-evolution equation (28), we can then utilize a generalization of Fuchs' algorithm [57]. For this, we determine the first $N_t = 32$ points in time using a Taylor expansion with a step size $\Delta t = 10^{-6}$, subsequently double the time step and numerically integrate the equations of motion, and repeat the duplication each time the next $N_t/2$ time points have been calculated.

B. Brownian dynamics simulations

As a proof of principle for our theory, we seek to predict the glassy behavior of a Kob-Andersen binary Lennard-Jones (LJ) mixture [30] of Brownian particles. This system consists of $N_A = 800$, $N_B = 200$ particles of type A and B, respectively. The position of each particle obeys (1), where we set $\zeta_{A,B} = \zeta_0 = 1.0$ (so that $D^A = D^B = k_B T/\zeta_0$ with k_B Boltzmann's constant and T the temperature), and the interaction forces are derived from the following interparticle potential:

$$V_{\alpha\beta}(r) = \begin{cases} 4\epsilon_{\alpha\beta}\left[\left(\frac{\sigma_{\alpha\beta}}{r}\right)^{12} - \left(\frac{\sigma_{\alpha\beta}}{r}\right)^{6} + C_{\alpha\beta}\right], & r \leqslant r^c_{\alpha\beta}, \\ 0, & r > r^c_{\alpha\beta}. \end{cases} \quad (35)$$

The interaction parameters, i.e., $\epsilon_{AA} = 1$, $\epsilon_{AB} = 1.5$, $\epsilon_{BB} = 0.5$, $\sigma_{AA} = 1$, $\sigma_{AB} = 0.8$, $\sigma_{BB} = 0.88$, are chosen to give good glass-forming mixtures and the constant $C_{\alpha\beta}$ fixes the potential to zero at the cutoff radius $r^c_{\alpha\beta} = 2.5\sigma_{\alpha\beta}$. Brownian dynamics simulations are then carried out using LAMMPS [58]. We impose periodic boundary conditions, fix the cubic box size to $L = 9.41\sigma_{AA}$ so that the number density equals $N/V = 1.2$, equilibrate the system at different temperatures, and afterwards track the particles over time. All results are presented in reduced units where σ_{AA}, ϵ_{AA}, ϵ_{AA}/k_B, and $\zeta_0\sigma^2_{AA}/\epsilon_{AA}$ represent the units of length, energy, temperature, and time, respectively [32].

Based on the simulation data, partial structure factors $S_{\alpha;\beta}(k)$ and intermediate scattering functions $F_{\alpha;\beta}(k, t)$ have been calculated for different temperatures up to two decimal numbers (values at more detailed temperatures are obtained via linear interpolation). The structure factors are rewritten in terms of an equidistant grid via cubic spline and polynomial extrapolation for the first two grid points. In combination with the set temperature (or diffusion coefficient) and number densities, they will then serve as input for the multicomponent GMCT equations, from which we find the corresponding theoretically predicted $F_{\alpha;\beta}(k, t)$ and $f_{\alpha;\beta}(k)$. In the following section we will discuss the effect of increasing the closure level $n_{\max}$ on the predicted dynamics, with a prime focus on the critical temperature, and we also compare our results to our own simulation results and previous (Brownian and Newtonian dynamics) simulations of the same system shown in Refs. [24,31–33,46].

IV. RESULTS & DISCUSSION

A. Nonergodicity parameter

Before proceeding to calculate the full dynamics, let us first focus on the long-time limit of the intermediate scattering functions $f_{\alpha;\beta}(k)$. These nonergodicity parameters serve as a convenient probe to find the critical temperature T_c at which an idealized glass transition occurs according to our theory. During such a transition the value of $f_{\alpha;\beta}(k)$ jumps discontinuously from zero to a finite value, indicating that the system never fully relaxes and ergodicity is broken. Solving Eqs. (31) and (33), and inspecting the resulting nonergodicity parameters allows us to retrieve the critical temperature, whose values (up to three decimal points) are listed for different closure levels in Figs. 1(a)–1(c). It can be seen that T_c decreases in value upon going to higher-order GMCT. In fact, when we plot the critical temperature as a function of $n_{\max}$ [see Fig. 1(d)], we may observe it moving and possibly converging towards the value $T^{\text{sim}}_c = 0.435$ obtained in both Newtonian and Brownian dynamics simulations [31–33]. To confirm a rigorous pattern of convergence, however, we must push our results towards larger values of $n_{\max}$, which so far has proved to be numerically demanding and is therefore left for future work.

Having specified the critical points, we now take a closer look at the details of the corresponding nonergodicity parameters, which are plotted for the relevant particle-type correlations in Figs. 1(a)–1(c). The curves show that for each correlation the nonergodicity parameter at the critical temperature retains a qualitatively similar shape for all considered closure levels. At the same time we observe a small quantitative increase of f^c_{AA} and f^c_{BB} for larger $n_{\max}$, which is consistent with the results of earlier work on single-component GMCT [22,26,27] and physically reflects a slowdown of the collective relaxation dynamics. To test how the predicted nonergodicity parameters compare to simulation results of the same system, we have also included the simulation data from Ref. [46] into Figs. 1(a)–1(c). It can be seen that the theoretically predicted nonergodicity parameters for each correlation and closure level are fairly consistent with the ones from simulation. Moreover, we note that increasing $n_{\max}$ initially yields quantitatively better results (especially for f^c_{AA}), although for the largest considered value of $n_{\max} = 3$ the agreement is already slightly worse, with GMCT overshooting the peak values. We mention that this overshooting of peak values has also been observed with respect to experimental results in previous work on single-component GMCT [26,27]. In a sense it reiterates the surprising ability of MCT to very accurately predict the nonergodicity parameters at a density or

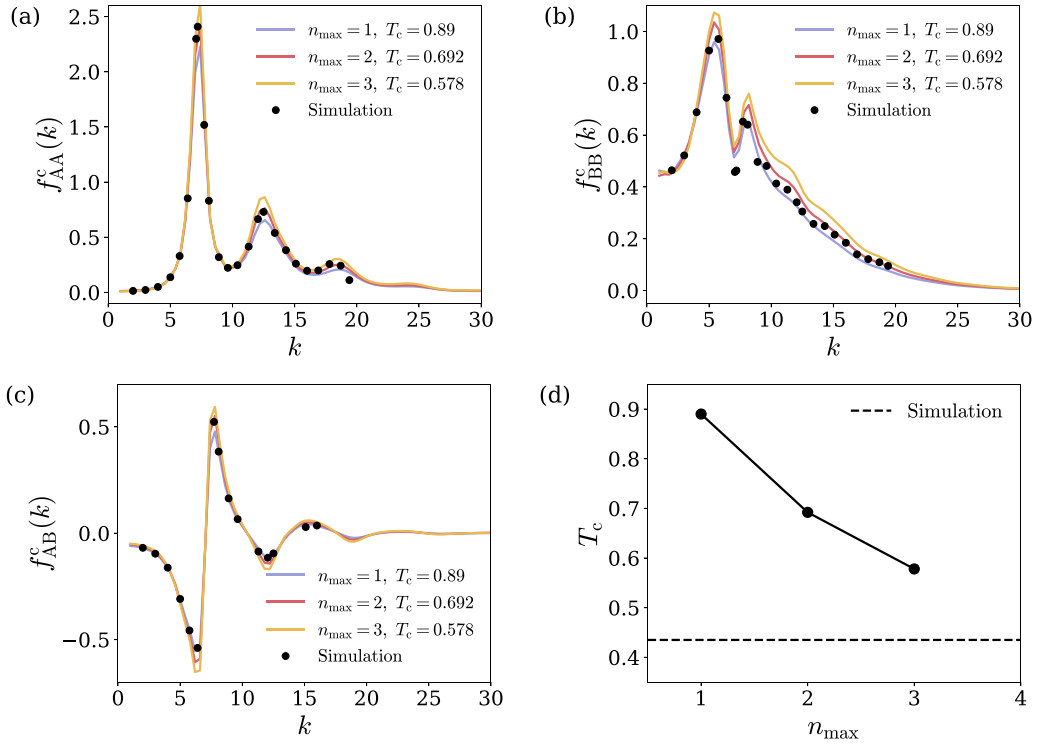

FIG. 1. [(a)–(c)] The critical nonergodicity parameters as a function of wave number k, calculated for different GMCT closures $n_{\max}$ at the respective critical temperatures T_c. The circles denote the simulation results from Ref. [46]. (d) The predicted critical temperature T_c as a function of closure level $n_{\max}$. Note that T_c decreases with increasing GMCT closure and seems to systematically move (and possibly converge) towards the value obtained in simulations, $T_c^{\text{sim}} = 0.435$ (dashed line).

temperature relatively far away from the true glass transition point. To better understand the quantitative disagreement of GMCT due to overshooting and test whether it proceeds in a convergent manner, akin to the observed decrease of the critical temperature, would require higher orders $n_{\max}$ to be included and a more accurate pinning down of the critical temperatures [22]; due to computational complexity, the critical temperature is here only determined up to three decimal numbers. Still, these results already suggest that extending the framework of GMCT from monodisperse towards multicomponent systems keeps its improved predictive power in terms of critical temperature intact and does not introduce any new qualitative flaws.

B. Dynamics and the relaxation time

Next, to study the effect of going to higher-order GMCT on the full dynamics of the system, we have also solved the time-dependent hierarchy of equations posed by Eqs. (28) and (30) for different closure levels $n_{\max}$ and temperatures T. The calculated intermediate scattering functions (for all particle-type correlations and normalized by the static structure factor) are shown for the first three closure levels and a subset of considered temperatures in Figs. 2 and 3. To illustrate the quantitatively improved predictive power of GMCT, we first focus on Fig. 2, where the temperature is kept fixed at a value of $T = 0.7$ and only the closure level has been varied. Being relatively far from the critical temperature $T_c^{\text{sim}} = 0.435$, one

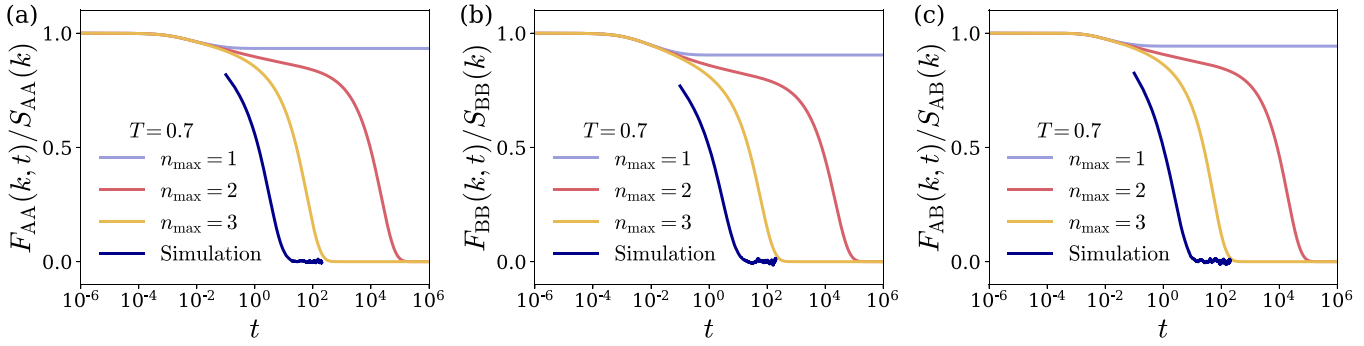

FIG. 2. Intermediate scattering functions as a function of time obtained directly from Brownian dynamics simulations or from binary GMCT. The latter results correspond to different closure levels. We have chosen a fixed temperature $T = 0.7$ and wave numbers $k = 7.4\sigma_{AA}^{-1}$ (a), $k = 5.8\sigma_{AA}^{-1}$ (b), and $k = 7.8\sigma_{AA}^{-1}$ (c) close to the first peak of $S_{\alpha\beta}(k)$.

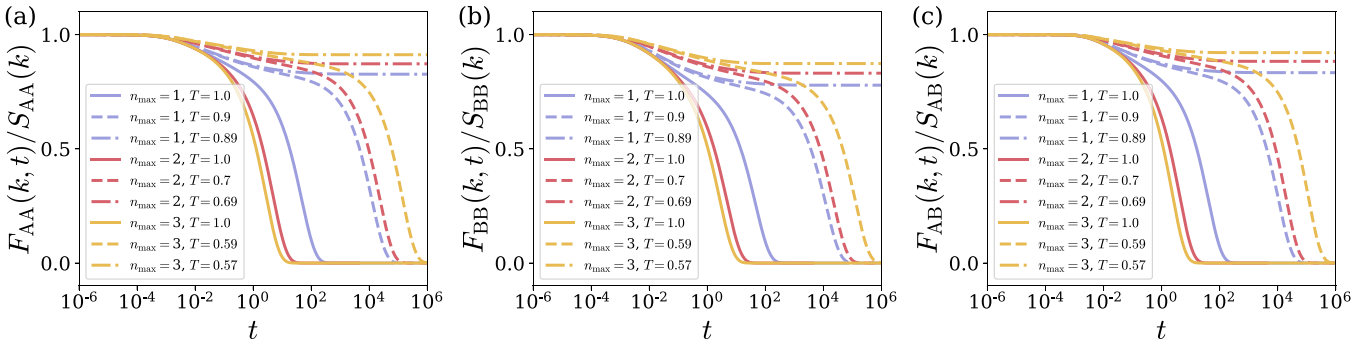

FIG. 3. Intermediate scattering functions as a function of time obtained from binary GMCT for different closure levels and different temperatures. We have chosen wave numbers $k = 7.4\sigma_{AA}^{-1}$ (a), $k = 5.8\sigma_{AA}^{-1}$ (b), and $k = 7.8\sigma_{AA}^{-1}$ (c) close to the first peak of $S_{\alpha\beta}(k)$.

expects a liquid state with the intermediate scattering function relaxing to zero at a timescale on the order of $\sim 10^1$ [32]. This is confirmed by our simulation results, which are also shown in Fig. 2. However, at this temperature standard MCT ($n_{max} = 1$) incorrectly predicts a nonergodic glassy state, evident from the fact that all components of $F_{\alpha\beta}(k,t)$ retain a plateau value and do not relax to zero. In comparison, second-order GMCT ($n_{max} = 2$) already correctly predicts a liquid state, although the timescale at which the two-point density correlation functions decay to zero is still overestimated with respect to the values obtained in simulations. This timescale is seen to be pushed back further towards its expected value upon moving to third-order GMCT ($n_{max} = 3$), thereby demonstrating how GMCT can systematically improve its predictions and possibly approach actual simulation results in the limit $n_{max} \to \infty$. Moreover, we may note that the systematic improvement occurs in almost the same fashion for each combination of particle types (either AA, BB, or AB).

We now proceed to the temperature dependence of the intermediate scattering functions, shown in Fig. 3. For all closure levels, it is apparent that the relaxation of each component of $F_{\alpha\beta}(k,t)$ takes an increasingly longer time upon cooling the system, until, at a small enough temperature, it fails to relax over the entire simulated time range. An inspection of the presented temperatures shows that the points at which the intermediate scattering functions cease to decay to zero are in agreement with the critical points obtained from the long-time-limit calculations. Additionally, we may observe that the overall shape of the relaxation curves is similar across all closure levels. This suggests that higher-order GMCT does not yield strong qualitative changes, and we expect the celebrated MCT scaling laws [14,16,56] to also hold for multicomponent GMCT. Note that this has already been rigorously shown for single-component GMCT [22,23].

We conclude our discussion by exploring one of such scaling laws, namely, the power law divergence of the relaxation time, for our binary LJ mixture. As an operational definition we follow Refs. [31,32] and let the relaxation time τ_α mark the point at which the intermediate scattering function has decreased to e^{-1} of its initial value, i.e., $F_{\alpha\beta}(k,\tau_\alpha)/S_{\alpha\beta}(k) = e^{-1}$ [with the wave number k corresponding to the first peak of $S_{\alpha\beta}(k)$]. When described as a function of the reduced temperature $\epsilon = (T - T_c)/T_c$, these relaxation times are expected to follow a power law divergence given by $\tau_\alpha \propto \epsilon^{-\gamma}$, with γ a critical exponent related to the fragility of the material. We have plotted the values of τ_α obtained directly from our Brownian dynamics simulations and the theoretically predicted ones for different closures in Fig. 4. It can be seen that for each component the theoretical results initially (down to $\epsilon \gtrsim 0.1$) follow a power law (represented by a straight line) before variations start to occur for the higher-order GMCT results. We believe that the observed deviations from a straight line when approaching the critical temperature (smaller ϵ) are a result of subtle inaccuracies in the static structure factors obtained from simulations. Since changes in the static structure factor are amplified for increasing order n_{max}, this can explain why deviations become more evident when we go beyond MCT, while for the latter an approximately straight line is retained over the full investigated window of reduced temperatures. Alternatively, it is also possible that our results are not fully converged yet with respect to the wave-number grid, which for computational reasons we have limited to $N_k = 100\ k$ points. Taking this into account, we have only fitted the relaxation times up to a value of $\epsilon \sim 0.1$, yielding for all particle-type correlations and closures an exponent between $\gamma \approx 2.3$ and 2.4. Fitting the simulation values for τ_α, which can also be seen to follow a straight line, we, for all considered cases, find an exponent between $\gamma \approx 2.3$ and 2.4. Overall, these values are in good agreement with each other and those retrieved in Refs. [31,32], and suggest that increasing the GMCT closure does not dramatically alter the critical exponent and thus the calculated fragility for this particular model system. In comparison, for a hard-sphere system, GMCT has been shown to predict a significant increase of the critical exponent [22].

V. CONCLUSION

In this work we have presented the first derivation of a fully time-dependent, microscopic, generalized MCT for colloidal mixtures obeying a many-body Smoluchowski equation. Our theory is inspired by earlier, time-independent GMCT studies on monodisperse colloidal systems MCT [26,27] and by previous work on time-dependent Newtonian GMCT [20,21,24]. The framework we put forward consists of a hierarchy of coupled integrodifferential equations describing the time dependence of diagonal density correlation functions of increasing order. For the first three entries, i.e., the two-, four-, and six-point density correlation functions, the corresponding equations of motion (and their dependence on the

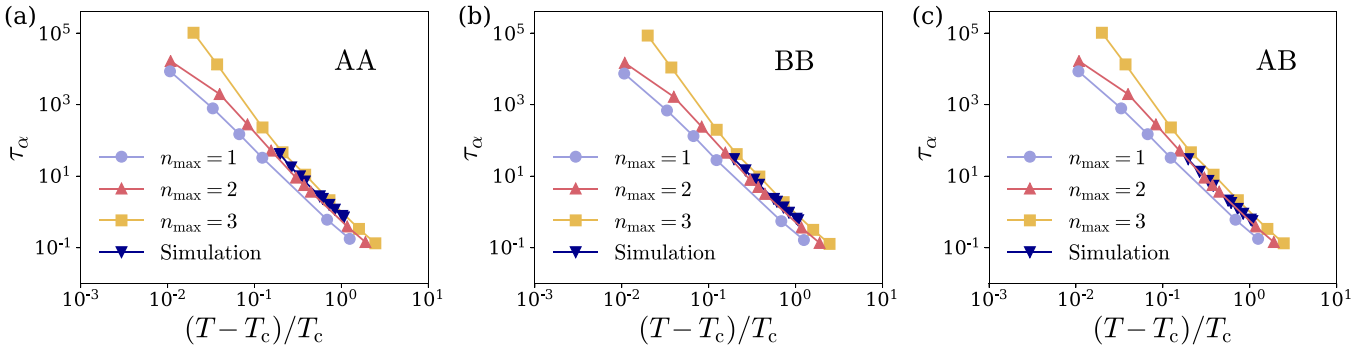

FIG. 4. The structural relaxation time corresponding to (a) AA, (b) BB, and (c) AB correlations as a function of the reduced temperature for different GMCT closure levels. The results obtained directly from Brownian dynamics simulations are also added for reference.

four-, six-, and eight-point density correlation functions, respectively) have been explicitly calculated. Subsequently, we have extrapolated this hierarchical construct to describe correlation functions of arbitrary order and thereby established our fully generalized MCT. Using only the partial static structure factors and no additional fit parameters as input, the hierarchy can be closed at an order n and subsequently solved self-consistently to retrieve the relaxation dynamics of a colloidal mixture and study its glassy behavior. Moreover, a careful inspection of the involved equations has shown that they, consistent with standard MCT, are *identical* to the ones obtained from Newtonian GMCT [24] when taking the overdamped limit. The nontrivial similarity between Brownian and Newtonian MCT is therefore maintained for our multicomponent GMCT, where we highlight that such an equivalency is also expected based on simulation results [24,31–33].

As an explorative demonstration of the theory, we have used it to predict the glassy behavior of a three-dimensional Kob-Andersen binary LJ mixture of Brownian particles. For such a system the theory yields an ergodicity-breaking (idealized glass) transition at decreasing critical temperatures upon increasing the closure level n_{max}. In particular, this decrease seems to occur (at least for the considered closure levels) in a convergent manner towards the actual experimental value obtained in both Newtonian and Brownian dynamics simulations. Additionally, a careful study of the calculated nonergodicity parameters and intermediate scattering functions suggests that no strong qualitative changes occur upon increasing the closure level, while quantitative improvements are observed. These results support the role of GMCT as a promising, systematically improvable, first-principles theory to study the dynamics of glass-forming materials.

Finally, we want to mention the recent heightened interest in active glassy materials where, besides exhibiting passive motion, the constituent particles are also able to autonomously move through the consumption of energy [2]. For such materials several active MCT theories have recently been put forward [59–66]. Since most model active systems are usually considered in the overdamped limit, e.g., active Brownian particles, our colloidal GMCT framework might also serve as a stepping stone for the development of active GMCT theories.

ACKNOWLEDGMENTS

We thank Professor Walter Kob for kindly providing us with the data of Ref. [46] for comparison. We acknowledge the Dutch Research Council (NWO) for financial support through a START-UP Grant (V.E.D., C.L., and L.M.C.J.) and Vidi grant (L.M.C.J.).

[1] L. M. C. Janssen, Front. Phys. **6**, 97 (2018).
[2] L. M. C. Janssen, J. Phys.: Condens. Matter **31**, 503002 (2019).
[3] L. Berthier and G. Biroli, Rev. Mod. Phys. **83**, 587 (2011).
[4] N. Klongvessa, F. Ginot, C. Ybert, C. Cottin-Bizonne, and M. Leocmach, Phys. Rev. Lett. **123**, 248004 (2019).
[5] N. Klongvessa, F. Ginot, C. Ybert, C. Cottin-Bizonne, and M. Leocmach, Phys. Rev. E **100**, 062603 (2019).
[6] J. Mattsson, H. M. Wyss, A. Fernandez-Nieves, K. Miyazaki, Z. Hu, D. R. Reichman, and D. A. Weitz, Nature (London) **462**, 83 (2009).
[7] T. E. Angelini, E. Hannezo, X. Trepat, M. Marquez, J. J. Fredberg, and D. A. Weitz, Proc. Natl. Acad. Sci. USA **108**, 4714 (2011).
[8] Y. Yang, J. Zhou, F. Zhu, Y. Yuan, D. J. Chang, D. S. Kim, M. Pham, A. Rana, X. Tian, Y. Yao, S. J. Osher, A. K. Schmid, L. Hu, P. Ercius, and J. Miao, Nature (London) **592**, 60 (2021).
[9] B. Li, K. Lou, W. Kob, and S. Granick, Nature (London) **587**, 225 (2020).
[10] A. R. Abate and D. J. Durian, Phys. Rev. E **76**, 021306 (2007).
[11] S. Ciarella, R. A. Biezemans, and L. M. C. Janssen, Proc. Natl. Acad. Sci. USA **116**, 25013 (2019).
[12] P. G. Debenedetti and F. H. Stillinger, Nature (London) **410**, 259 (2001).
[13] M. D. Ediger, C. A. Angell, and S. S. R. Nagel, J. Phys. Chem. **100**, 13200 (1996).
[14] W. Götze, *Complex Dynamics of Glass-Forming Liquids: A Mode-Coupling Theory* (Oxford University Press, Oxford, England, 2008).
[15] W. Götze and L. Sjogren, Rep. Prog. Phys. **55**, 241 (1992).
[16] D. R. Reichman and P. Charbonneau, J. Stat. Mech.: Theory Exp. (2005) P05013.
[17] W. Götze, J. Phys. Conden. Matter **11**, A1 (1999).

[18] F. Weysser, A. M. Puertas, M. Fuchs, and T. Voigtmann, Phys. Rev. E **82**, 011504 (2010).
[19] L. M. C. Janssen, P. Mayer, and D. R. Reichman, Phys. Rev. E **90**, 052306 (2014).
[20] L. M. C. Janssen and D. R. Reichman, Phys. Rev. Lett. **115**, 205701 (2015).
[21] L. M. C. Janssen, P. Mayer, and D. R. Reichman, J. Stat. Mech.: Theory Exp. (2016) 054049.
[22] C. Luo and L. M. C. Janssen, J. Chem. Phys. **153**, 214507 (2020).
[23] C. Luo and L. M. C. Janssen, J. Chem. Phys. **153**, 214506 (2020).
[24] S. Ciarella, C. Luo, V. E. Debets, and L. M. C. Janssen, Eur. Phys. J. E **44**, 91 (2021).
[25] P. Mayer, K. Miyazaki, and D. R. Reichman, Phys. Rev. Lett. **97**, 095702 (2006).
[26] G. Szamel, Phys. Rev. Lett. **90**, 228301 (2003).
[27] J. Wu and J. Cao, Phys. Rev. Lett. **95**, 078301 (2005).
[28] C. Luo, V. E. Debets, and L. M. C. Janssen, J. Chem. Phys. **155**, 034502 (2021).
[29] G. Nägele, J. Bergenholtz, and J. Dhont, J. Chem. Phys. **110**, 7037 (1999).
[30] W. Kob and H. C. Andersen, Phys. Rev. Lett. **73**, 1376 (1994).
[31] L. Berthier and G. Tarjus, Phys. Rev. E **82**, 031502 (2010).
[32] E. Flenner and G. Szamel, Phys. Rev. E **72**, 031508 (2005).
[33] M. Nauroth and W. Kob, Phys. Rev. E **55**, 657 (1997).
[34] G. Nägele, Phys. Rep. **272**, 215 (1996).
[35] G. Tarjus and D. Kivelson, J. Chem. Phys. **103**, 3071 (1995).
[36] Z. Shi, P. G. Debenedetti, and F. H. Stillinger, J. Chem. Phys. **138**, 12A526 (2013).
[37] S. K. Kumar, G. Szamel, and J. F. Douglas, J. Chem. Phys. **124**, 214501 (2006).
[38] H. Mori, Prog. Theor. Phys. **33**, 423 (1965).
[39] R. Zwanzig, J. Chem. Phys. **33**, 1338 (1960).
[40] B. Cichocki and W. Hess, Physica A **141**, 475 (1987).
[41] K. Kawasaki, Physica A **215**, 61 (1995).
[42] See Supplemental Material at http://link.aps.org/supplemental/10.1103/PhysRevE.104.065302 for additional derivations.
[43] G. Szamel and H. Löwen, Phys. Rev. A **44**, 8215 (1991).
[44] G. Szamel and E. Flenner, EPL (Europhys. Lett.) **101**, 66005 (2013).
[45] H. W. Jackson and E. Feenberg, Rev. Mod. Phys. **34**, 686 (1962).
[46] F. Sciortino and W. Kob, Phys. Rev. Lett. **86**, 648 (2001).
[47] W. Kob, M. Nauroth, and F. Sciortino, J. Non-Cryst. Solids **307-310**, 181 (2002).
[48] A. Banerjee, S. Sengupta, S. Sastry, and S. M. Bhattacharyya, Phys. Rev. Lett. **113**, 225701 (2014).
[49] Z. E. Dell and K. S. Schweizer, Phys. Rev. Lett. **115**, 205702 (2015).
[50] F. P. Landes, G. Biroli, O. Dauchot, A. J. Liu, and D. R. Reichman, Phys. Rev. E **101**, 010602 (2020).
[51] B. Charbonneau, P. Charbonneau, and G. Szamel, J. Chem. Phys. **148**, 224503 (2018).
[52] R. A. Biezemans, S. Ciarella, O. Çaylak, B. Baumeier, and L. M. C. Janssen, J. Stat. Mech.: Theory Exp. (2020) 103301.
[53] L. F. Elizondo-Aguilera and T. Voigtmann, Phys. Rev. E **100**, 042601 (2019).
[54] N. Bidhoodi and S. P. Das, Phys. Rev. E **98**, 032126 (2018).
[55] S. Mandal, T. Franosch, and T. Voigtmann, Soft Matter **14**, 9153 (2018).
[56] T. Franosch, M. Fuchs, W. Götze, M. R. Mayr, and A. P. Singh, Phys. Rev. E **55**, 7153 (1997).
[57] M. Fuchs, W. Götze, I. Hofacker, and A. Latz, J. Phys.: Condens. Matter **3**, 5047 (1991).
[58] S. Plimpton, J. Comput. Phys. **117**, 1 (1995).
[59] A. Liluashvili, J. Ónody, and T. Voigtmann, Phys. Rev. E **96**, 062608 (2017).
[60] G. Szamel, J. Chem. Phys. **150**, 124901 (2019).
[61] G. Szamel, Phys. Rev. E **93**, 012603 (2016).
[62] M. Feng and Z. Hou, Soft Matter **13**, 4464 (2017).
[63] M. Feng and Z. Hou, Chin. J. Chem. Phys. **31**, 584 (2018).
[64] J. Reichert, L. F. Granz, and T. Voigtmann, Eur. Phys. J. E **44**, 27 (2021).
[65] T. F. F. Farage and J. M. Brader, arXiv:1403.0928.
[66] J. Reichert, S. Mandal, and T. Voigtmann, Phys. Rev. E **104**, 044608 (2021).